

# Simulation of square-root processes made simple: applications to the Heston model

Eduardo Abi Jaber\*

Ecole Polytechnique, CMAP

June 18, 2025

## Abstract

We introduce a simple, efficient and accurate numerical scheme that preserves non-negativity for simulating the square-root process. The novel idea is to simulate the integrated square-root process first instead of the square-root process itself. Numerical experiments on realistic parameter sets, applied for the integrated process and the Heston model, display high precision with a very low number of time steps. As a bonus, our scheme yields the exact limiting Inverse Gaussian distributions of the integrated square-root process with only one single time-step in two scenarios: (i) for high mean-reversion and volatility-of-volatility regimes, regardless of maturity; and (ii) for long maturities, independent of the other parameters.

## Introduction

Square-root processes are a cornerstone of stochastic modeling in finance, playing a central role in applications such as interest rates (Cox, Ingersoll Jr, and Ross, 1985), credit risk (Duffie and Singleton, 2012) and volatility (Heston, 1993). Despite their foundational importance, their simulation is often perceived as notoriously challenging. This work demonstrates that this perception is unwarranted by presenting an extremely simple, accurate and nonnegative preserving discretization scheme. The core idea is to simulate the integrated process first instead of the process itself.

The square-root process  $V$  is of the form:

$$V_t = V_0 + \int_0^t (a + bV_s) ds + c \int_0^t \sqrt{V_s} dW_s, \quad (0.1)$$

where  $V_0, a \geq 0, b, c \in \mathbb{R}$ , and  $W$  is a standard Brownian motion.

The process exhibits an affine structure, meaning that both the instantaneous drift and the squared instantaneous diffusion are affine functions of  $V$ . This structure presents a double-edged sword:

- **Tractability for pricing:** The affine structure leads to a semi-analytical solution for the characteristic function, and opens the door to efficient Fourier-based option pricing methods, see Cox, Ingersoll Jr, and Ross (1985); Duffie, Filipović, and Schachermayer (2003); Heston (1993) and more generally Duffie, Filipović, and Schachermayer (2003).

---

\*eduardo.abi-jaber@polytechnique.edu. I am grateful for the financial support from the Chaires FiME-FDD, Financial Risks, Deep Finance & Statistics and Machine Learning and systematic methods in finance at Ecole Polytechnique. I would like to thank Aurélien Alfonsi, Elie Attal, Nathan De Carvalho, Louis-Amand Gérard, Shaun Li and Dimitri Sotnikov for fruitful discussions, as well as two anonymous referees for their valuable feedback.

- **Simulation challenges:** The same affine structure introduces a square-root term in the diffusion coefficient, posing numerical challenges, especially in maintaining the non-negativity of a discretized version of  $V$  of Euler-Maruyama type.

**Literature review.** There is a substantial body of literature on the simulation of square-root processes. To describe them, we define the time-integrated process  $U$  and the Brownian-integrated process  $Z$  by

$$U_{s,t} := \int_s^t V_r dr, \quad Z_{s,t} := \int_s^t \sqrt{V_r} dW_r, \quad s \leq t. \quad (0.2)$$

Despite differences in the proposed schemes, the approaches generally follow these steps:

- Step 1: Update  $V_{t_{i+1}}$  given  $V_{t_i}$ .
- Step 2: Sample  $U_{t_i, t_{i+1}}$  knowing  $(V_{t_i}, V_{t_{i+1}})$ .
- Step 3: Deduce  $Z_{t_i, t_{i+1}}$  using (0.1), by setting:

$$Z_{t_i, t_{i+1}} = \frac{1}{c} (V_{t_{i+1}} - V_{t_i} - a(t_{i+1} - t_i) - bU_{t_i, t_{i+1}}).$$

The schemes in the literature can be broadly categorized as follows:

**Category 1 - dynamics-based:** Methods that update  $V_{t_{i+1}}$  knowing  $V_{t_i}$  in Step 1 using (improved) Euler-Maruyama-type discretizations of the stochastic differential equation of  $V$  in (0.1). And then approximate the integral  $U_{t_i, t_{i+1}}$  from  $(V_{t_i}, V_{t_{i+1}})$  in Step 2 using for instance left-point or mid-point rule. The advantage of such methods is usually their relative simplicity and interpretability. This category includes the works of [Alfonsi \(2005, 2010\)](#); [Berkaoui, Bossy, and Diop \(2008\)](#); [Deelstra and Delbaen \(1998\)](#); [Gyöngy and Rásónyi \(2011\)](#); [Higham and Mao \(2005\)](#); [Kahl and Jäckel \(2006\)](#); [Neuenkirch and Szpruch \(2014\)](#) among many others. A limitation of this category is that not all Euler-type methods preserve the non-negativity of  $V$  and can sometimes introduce important biases.

**Category 2 - distribution-based:** Methods that sample  $V_{t_{i+1}}$  knowing  $V_{t_i}$  in Step 1 using its exact (or approximate) distribution, which is a noncentral chi-squared distribution, which is relatively efficient numerically. And then sample  $U_{t_i, t_{i+1}}$  based on either the exact or (approximate) distribution of  $U_{t_i, t_{i+1}}$  conditional on the endpoints  $(V_{t_i}, V_{t_{i+1}})$ . Simulating from the exact distribution is possible as shown by [Broadie and Kaya \(2006\)](#), however it is computationally expensive. Later works initiated by [Glasserman and Kim \(2011\)](#) introduced approximations to improve efficiency. Techniques such as matching moments coupled with educated guesses of the conditional distribution of  $U_{t_i, t_{i+1}}$  on  $(V_{t_i}, V_{t_{i+1}})$  have been proposed: with an Inverse Gaussian distribution by [Tse and Wan \(2013\)](#), Inverse Gamma distribution by [Bégin, Bédard, and Gaillardetz \(2015\)](#), Poisson conditioning of [Choi and Kwok \(2024\)](#) distributions, discrete random variables by [Lileika and Mackevičius \(2020\)](#). These methods offer a good trade-off between computational time and accuracy, but they usually require some amount of offline/online pre-computations and lack transparency in their mathematical link with the dynamics in (0.1).

In some cases, both categories are combined in different steps. The most notable example is the Quadratic Exponential (QE) scheme developed by [Andersen \(2008\)](#) which samples  $V_{t_{i+1}}$  knowing  $V_{t_i}$  using a switching between a squared Gaussian (when  $V_{t_i}$  is large enough) or a tweaked exponential distribution (when  $V_{t_i}$  is small) with moment matching for Step 1; and then uses the mid-point rule to approximate  $U_{t_i, t_{i+1}}$  by  $(V_{t_i} + V_{t_{i+1}})/2$  in Step 2. Despite its hybrid nature, the methodology still adheres to the conventional structure of Steps 1, 2, and 3. The QE scheme seems

quite popular among practitioners and plays the role of a benchmark in the academic literature. In the same vein, [Zhu \(2011\)](#) approximates the volatility process, rather than the variance process, using an Ornstein-Uhlenbeck process with moment matching. [Van Haastrecht and Pelsser \(2010\)](#) proposes various hybrid approaches to accelerate the discretizations of Steps 1 and 2. Finally, we also mention the comparison study in [Possamaï and Gauthier \(2011\)](#).

While these methodologies are typically treated as distinct, there has been limited investigation into the connections between the dynamics-based and distributional approaches. In a perfect world, one would like to read-off the distributional properties from Euler-type discretization method. This work aims to bridge that gap by establishing a clear link between discretized dynamics and distributional properties, thereby offering a deeper understanding of the underlying affine dynamics.

This work aims to reconcile the affine structure with Euler-Maruyama simulation schemes. Specifically, we ask:

*Is there an unexplored way to exploit the affine structure for discretizing the process in an Euler-Maruyama fashion?*

*Can we construct a simple, efficient, and accurate scheme for simulating square-root processes?*

We answer these questions *affirmatively*.

**Main contributions.** Our approach builds upon simulating the integrated quantities (0.2) first before the process  $V$ . These quantities not only capture the essential information required for many financial applications but are also critical for simulating other processes, such as the [Heston \(1993\)](#) model.

We already have all the ingredients needed to present the discretization scheme we propose, which emphasizes the simplicity of the approach. The following algorithm recursively constructs  $(\widehat{V}_i)_{i=0,\dots,n}$ ,  $(\widehat{U}_{i,i+1})_{i=0,\dots,n-1}$ , and  $(\widehat{Z}_{i,i+1})_{i=0,\dots,n-1}$ . We coin it the **iVi** scheme for **integrated  $\mathbf{V}$**  (or **V**ariance) **implicit** scheme.

---

**Algorithm 1 - The iVi scheme:** Simulation of  $\widehat{V}, \widehat{U}, \widehat{Z}$

---

- 1: **Input:** Initial value  $\widehat{V}_0 = V_0$ , partition  $0 = t_0 < t_1 < \dots < t_n = T$ , parameters  $a, b, c$ .
- 2: **Output:**  $\widehat{V}_{i+1}, \widehat{U}_{i,i+1}, \widehat{Z}_{i,i+1}$  for  $i = 0, \dots, n - 1$ .
- 3: **for**  $i = 0$  to  $n - 1$  **do**
- 4:     Compute the quantities:

$$\alpha_i = \widehat{V}_i \frac{e^{b(t_{i+1}-t_i)} - 1}{b} + \frac{a}{b} \left( \frac{e^{b(t_{i+1}-t_i)} - 1}{b} - (t_{i+1} - t_i) \right), \quad \sigma_i = c \frac{e^{b(t_{i+1}-t_i)} - 1}{b}. \quad (0.3)$$

- 5:     Simulate the increment of the integrated process:

$$\widehat{U}_{i,i+1} \sim IG \left( \alpha_i, \left( \frac{\alpha_i}{\sigma_i} \right)^2 \right). \quad (0.4)$$

- 6:     Set:

$$\widehat{Z}_{i,i+1} = \frac{1}{\sigma_i} \left( \widehat{U}_{i,i+1} - \alpha_i \right) \quad (0.5)$$

- 7:     Update the instantaneous process:

$$\widehat{V}_{i+1} = \widehat{V}_i + a(t_{i+1} - t_i) + b\widehat{U}_{i,i+1} + c\widehat{Z}_{i,i+1}. \quad (0.6)$$

- 8: **end for**
-

Here,  $IG$  refers to an Inverse Gaussian distribution, whose definition and a simple sampling algorithm are provided in Appendix A and with the convention in (0.3) that for  $b = 0$ :  $\frac{e^{bt}-1}{b} = t$  and  $\frac{e^{bt}-1}{b} - t = \frac{t^2}{2}$ .

Aside from the inherent simplicity of Algorithm 1, which is both efficient and free from precomputations and fine-tuning of hyperparameters, we show that the iVi scheme enjoys the following key features:

- The scheme is built from straightforward right-endpoint Euler-type discretization rule applied to a single integral in the dynamics of  $U$  and leverages the affine structure on the level of the dynamics of  $(U, Z)$ .
- The scheme ensures the non-negativity of the process  $V$ , i.e.,  $\widehat{V}_i \geq 0$  for all  $i = 0, \dots, n$ , as established in Theorem 1.3.
- The scheme captures essential distributional properties:
  - (i) The first conditional moments are perfectly captured, as proved in Proposition 1.4.
  - (ii) The Inverse Gaussian distribution emerges naturally from the right-endpoint discretization of the conditional characteristic function of  $U$ , as shown in Remark 1.6.
  - (iii) The scheme accurately reproduces the Inverse Gaussian limiting distribution of  $U_{0,T}$  in market regimes characterized by large mean reversion and high volatility of volatility, in line with the first observations made by Mechkov (2015) and the works of Abi Jaber and De Carvalho (2024); McCrickerd (2019), see Remark 1.7.
  - (iv) It also provides the exact Inverse Gaussian limiting distribution of  $U_{0,T}$  for large maturities, as established by Forde and Jacquier (2011), Remark 1.7.
- In terms of performance, the iVi scheme displays high precision with very few time-steps, for the integrated process and the Heston model, even under realistic and challenging scenarios, see Sections 2 and 3. As illustration, Figure 1 provides six slices of the volatility surface in the Heston model (black) with challenging parameters calibrated to the market. Our iVi scheme (in orange) is computed with only one single time step (equal to the maturity  $T$ ) per slice!

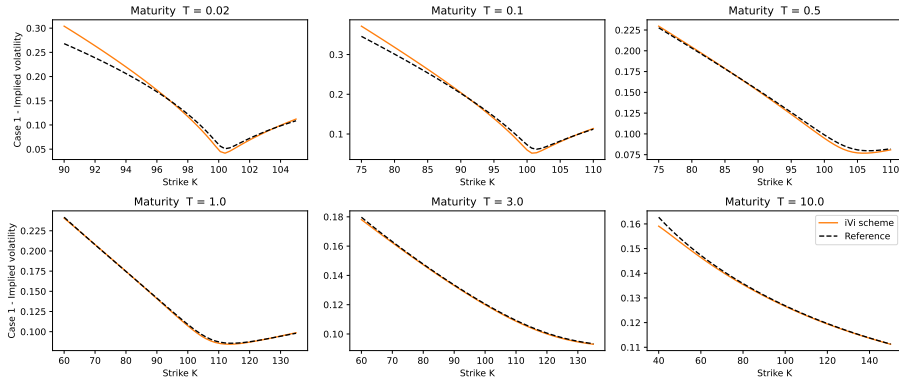


Figure 1: Heston's Implied volatility surface with the iVi scheme with one single time step and 2 million sample paths for model parameters as in Case 1 in Table 1.

**Our approach.** Unlike the conventional methodology, our approach departs from the usual Step 1, 2, and 3 order. Instead of first sampling  $V_{t_{i+1}}$ , we focus on sampling  $U_{t_i, t_{i+1}}$  given  $V_{t_i}$  by discretizing the dynamics of  $U$  using a simple Euler-Maruyama right-endpoint scheme. Leveraging

the affine structure, we derive an intertwined relationship between  $U_{t_i, t_{i+1}}$  and  $Z_{t_i, t_{i+1}}$  in the form of the implicit equation:

$$U_{t_i, t_{i+1}} \approx \alpha_i + \sigma_i Z_{t_i, t_{i+1}}, \quad \text{and} \quad [Z]_{t_i, t_{i+1}} = U_{t_i, t_{i+1}},$$

where  $[\cdot]$  denotes the quadratic variation.

A solution (among many) to this equation is given by an Inverse Gaussian distribution, leading to the sampling formula in (0.4). Using this relationship, the definition of  $Z_{t_i, t_{i+1}}$  in (0.5) becomes clear, and the update of  $V_{t_{i+1}}$  in (0.6) follows naturally from the dynamics (0.1). To justify the choice of the Inverse Gaussian distribution, we exploit the expression of the characteristic function of  $U_{t_i, t_{i+1}}$  given  $V_{t_i}$  in terms of Riccati equations. We demonstrate that applying the same right-endpoint rule at the level of the Riccati equations naturally leads to an Inverse Gaussian distribution.

This novel perspective not only simplifies the simulation process but also provides deeper insights, which might be useful in other contexts, into the interplay between the dynamics and distributional properties of the square-root process—or more precisely, of the integrated square-root process!

**Outline.** In Section 1 we provide the mathematical derivation of the scheme as well as its distributional properties. Numerical illustrations for the scheme for the integrated process  $U$  and the Heston model are provided in Sections 2 and 3. Useful properties of Inverse Gaussian distribution and the Heston model are collected in the appendices, together with calibrated volatility surfaces for the parameters used in our experiments.

## 1 The iVi scheme

In this section, we will detail the mathematical derivation of the iVi scheme, prove that it preserves non-negativity for the discretized process  $\hat{V}$  and study some of its distributional properties.

### 1.1 Deriving the iVi scheme: one integral to approximate

The first step is to write the dynamics of the integrated process  $U_{s,t} = \int_s^t V_r dr$  between  $s$  and  $t$ . This is done by first writing the variation of constants formula for the process  $V$  in (0.1) as

$$V_r = V_s e^{b(r-s)} + a \frac{e^{b(r-s)} - 1}{b} + c \int_s^r e^{b(r-u)} dZ_{s,u}, \quad s \leq r, \quad (1.1)$$

where  $dZ_{s,u}$  is the differential with respect to the second variable  $u$ , for  $u \geq s$ , i.e.  $dZ_{s,u} = \sqrt{V_u} dW_u$ . Integrating  $V_r$  between  $s$  and  $t$  and applying stochastic Fubini's theorem yields the following dynamics for  $U$ .

**Proposition 1.1.** *The dynamics of the process  $U$  defined in (0.2) are given by*

$$U_{s,t} = V_s \frac{e^{b(t-s)} - 1}{b} + a \left( \frac{e^{b(t-s)} - 1}{b} - (t-s) \right) + c \int_s^t e^{b(t-r)} Z_{s,r} dr, \quad s \leq t, \quad (1.2)$$

where we recall the convention that for  $b = 0$ :  $\frac{e^{bt} - 1}{b} = t$  and  $\frac{\frac{e^{bt} - 1}{b} - t}{2} = \frac{t^2}{2}$ .

*Proof.* Fix  $s \leq t$ . Integrating the dynamics of  $V$  in (1.1) between  $s$  and  $t$  gives

$$U_{s,t} = \int_s^t V_r dr = V_s \frac{e^{b(t-s)} - 1}{b} + a \left( \frac{e^{b(t-s)} - 1}{b} - (t-s) \right) + c \int_s^t \int_s^r e^{b(r-u)} dZ_{s,u} dr.$$

Successive applications of stochastic Fubini's theorem and a change of variables (using that  $Z_{s,s} = 0$ ), on the last term yield

$$\begin{aligned}
\int_s^t \int_s^r e^{b(r-u)} dZ_{s,u} dr &= \int_s^t \int_u^t e^{b(r-u)} dr dZ_{s,u} \\
&= \int_s^t \int_0^{t-u} e^{bv} dv dZ_{s,u} \\
&= \int_0^{t-s} \int_s^{t-v} dZ_{s,u} e^{bv} dv \\
&= \int_0^{t-s} Z_{s,t-v} e^{bv} dv \\
&= \int_s^t Z_{s,u} e^{b(t-u)} du,
\end{aligned}$$

which ends the proof.  $\blacksquare$

The main idea behind our scheme is to simply discretize the equation (1.2) for the integrated process  $U$  between  $t_i$  and  $t_{i+1}$ , assuming the knowledge of  $\hat{V}_i \approx V_{t_i}$ . There is only one integral to discretize. Using the right endpoint rule on  $Z_{t_i, \cdot}$ , i.e. approximating  $Z_{t_i, s}$  by the value  $Z_{t_i, t_{i+1}}$  for  $s \in [t_i, t_{i+1})$ , yields

$$\int_{t_i}^{t_{i+1}} e^{b(t_{i+1}-r)} Z_{t_i, r} dr \approx \int_{t_i}^{t_{i+1}} e^{b(t_{i+1}-r)} dr Z_{t_i, t_{i+1}} = \frac{e^{b(t_{i+1}-t_i)} - 1}{b} Z_{t_i, t_{i+1}}.$$

Plugging this in (1.2), yields

$$U_{t_i, t_{i+1}} \approx \hat{V}_i \frac{e^{b(t_{i+1}-t_i)} - 1}{b} + \frac{a}{b} \left( \frac{e^{b(t_{i+1}-t_i)} - 1}{b} - (t_{i+1} - t_i) \right) + c \frac{e^{b(t_{i+1}-t_i)} - 1}{b} Z_{t_i, t_{i+1}}. \quad (1.3)$$

Now the key point is to observe that this forms an implicit equation on  $U_{t_i, t_{i+1}}$  by rewriting  $Z$  using a time-changed Brownian motion. Indeed, recall from the definition of  $(Z_{t_i, s})_{s \geq t_i}$  in (0.2) that it is a continuous local martingale with quadratic variation  $\int_{t_i}^{\cdot} V_r dr = U_{t_i, \cdot}$ . Hence, an application of the celebrated Dambis, Dubins-Schwarz Theorem see (Revuz and Yor, 2013, Theorem 1.1.6) yields the representation of  $(Z_{t_i, s})_{s \geq t_i}$  in terms of a time changed Brownian motion  $Z_{t_i, s} = \tilde{W}_{U_{t_i, s}}$  for all  $s \geq t_i$  where  $\tilde{W}$  is a standard Brownian motion.

Hence, plugging this in (1.3), approximating  $U_{t_i, t_{i+1}}$  boils down to finding a nonnegative random variable  $\hat{U}_{i, i+1}$  solving

$$\hat{U}_{i, i+1} = \alpha_i + \sigma_i \tilde{W}_{\hat{U}_{i, i+1}}, \quad (1.4)$$

with  $\alpha_i$  and  $\sigma_i$  as in (0.3).

Said differently  $\hat{U}_{i, i+1}$  is a passage time of the level  $\alpha_i$  for the drifted Brownian motion  $(s - \sigma_i \tilde{W}_s)_{s \geq 0}$ . In particular, the first passage time

$$X = \inf \left\{ s \geq 0 : s - \sigma_i \tilde{W}_s = \alpha_i \right\}$$

satisfies (1.4). It is well known that  $X$  follows an Inverse Gaussian distribution  $IG(\mu_i, \lambda_i)$  with mean parameter  $\mu_i = \alpha_i$  and shape parameter  $\lambda_i = \frac{\alpha_i^2}{\sigma_i^2}$ . Inverse Gaussian distributions are recalled in Appendix A.

Hence, we sample  $\hat{U}_{i, i+1}$  using the Inverse Gaussian distribution as in (0.4). Beyond its tractability and efficient sampling, see Algorithm 2, the choice of the Inverse Gaussian distribution is further

justified in Section 1.3.2 where it is shown to be intimately linked with the distributional properties of the integrated square-root process  $U$ . Then, using (1.4) we can define the  $\widehat{Z}_{i,i+1}$  (which plays the role of  $\widehat{W}_{\widehat{U}_{i,i+1}}$ ) using equation (0.5). Finally, to update  $\widehat{V}$ , we write the square-root equation (0.1) between  $t_i$  and  $t_{i+1}$  as

$$V_{t_{i+1}} = V_{t_i} + a(t_{i+1} - t_i) + bU_{t_i, t_{i+1}} + cZ_{t_i, t_{i+1}}.$$

This yields the update formula for  $\widehat{V}_{i,i+1}$  in (0.6) follows.

Putting everything together, we arrive at the iVi scheme of Algorithm 1.

**Remark 1.2.** *A simpler scheme can be derived without using the variation of constants formula (0.1), after a simple integration of the equation (0.1) for  $V$  between  $s$  and  $t$ , to get*

$$U_{s,t} = V_s(t-s) + a\frac{(t-s)^2}{2} + \int_s^t (bU_{s,r} + cZ_{s,r}) dr. \quad (1.5)$$

Using the right endpoint to approximate the integral between  $t_i$  and  $t_{i+1}$  in (1.5), we arrive to the implicit scheme

$$U_{i,i+1} = V_i(t_{i+1} - t_i) + a\frac{(t_{i+1} - t_i)^2}{2} + b(t_{i+1} - t_i)U_{i,i+1} + c(t_{i+1} - t_i)Z_{i,i+1}.$$

Hence, as long as  $(1 - b(t_{i+1} - t_i)) > 0$  (which is the case for mean reverting dynamics, i.e.  $b \leq 0$ ), using the same ideas as above we get to

$$\widetilde{U}_{i,i+1} \sim IG\left(\frac{\widetilde{\alpha}_i}{(1 - b(t_{i+1} - t_i))}, \left(\frac{\widetilde{\alpha}_i}{\widetilde{\sigma}_i}\right)^2\right),$$

with

$$\widetilde{\alpha}_i = \widetilde{V}_i(t_{i+1} - t_i) + a\frac{(t_{i+1} - t_i)^2}{2}, \quad \widetilde{\sigma}_i = c(t_{i+1} - t_i),$$

and

$$\widetilde{Z}_{i,i+1} = \frac{1}{\widetilde{\sigma}_i} \left( (1 - b(t_{i+1} - t_i))\widetilde{U}_{i,i+1} - \widetilde{\alpha}_i \right).$$

Then,  $\widetilde{V}_{i+1}$  is updated using (0.6) but with  $(\widetilde{V}, \widetilde{U}, \widetilde{Z})$  instead of  $(\widehat{V}, \widehat{U}, \widehat{Z})$ . It should be clear that such scheme introduces an additional bias compared to Algorithm 1 since, the drift here is approximated instead of being exactly solved for, using the variation of constants formula. ■

## 1.2 Well-definedness and non-negativity of $\widehat{V}$

To ensure the well-definedness of Algorithm 1, we still have to check that the mean parameter  $\alpha_i$  in (0.3) of the Inverse Gaussian distribution is nonnegative for each  $i = 0, \dots, n$ , with the convention that  $IG(0, 0)$  is equal to 0. This is the object of the next theorem, and as a by-product, we will obtain that the discretized square-root process  $\widehat{V}$  satisfies  $\widehat{V}_i \geq 0$  for all  $i = 0, \dots, n$ .

**Theorem 1.3.** *Let  $V_0, a \geq 0$  and  $b, c \in \mathbb{R}$ . Consider  $(\widehat{V}_i)_{i=0, \dots, n}$ ,  $(\widehat{U}_{i,i+1})_{i=0, \dots, n-1}$ , and  $(\widehat{Z}_{i,i+1})_{i=0, \dots, n-1}$  satisfying the recursions of the iVi scheme in Algorithm 1. Then, we have that*

$$\widehat{V}_i, \alpha_i \geq 0, \quad i = 0, \dots, n.$$

*Proof.* Since  $a \geq 0$ , it follows from the definition of  $\alpha_i$  in (0.3) that  $\alpha_i \geq 0$  if  $\widehat{V}_i \geq 0$ , for all  $i = 0, \dots, n$ . Hence, it suffices to prove that

$$\widehat{V}_i \geq 0, \quad i = 0, \dots, n.$$

First we note that for  $i = 0$ , we have that  $\widehat{V}_0 = V_0 \geq 0$  by definition of  $V_0$ . Fix  $i = 0, \dots, n-1$ , let us show that  $\widehat{V}_{i+1} \geq 0$  using (0.6). Plugging in (0.6), the expression for  $Z_{i,i+1}$  given by (0.5) and that of  $\alpha_i$  in (0.3), we arrive to

$$V_{i+1} = \frac{be^{b(t_{i+1}-t_i)}}{e^{b(t_{i+1}-t_i)} - 1} U_{i,i+1} + \frac{a}{b} \left[ \frac{b(t_{i+1}-t_i)e^{b(t_{i+1}-t_i)}}{e^{b(t_{i+1}-t_i)} - 1} - 1 \right]$$

the first term is nonnegative for all  $b \in \mathbb{R}$ , since  $U_{i,i+1} \geq 0$  by definition of an Inverse Gaussian distribution and the second term is also nonnegative by using that  $a \geq 0$  and observing that the function  $f(x) := \frac{xe^x}{e^x - 1}$  satisfies  $f(x) \leq 1$  for  $x \leq 0$  and  $f(x) \geq 1$  for  $x \geq 0$  so that  $\frac{1}{b}(f(b(t_{i+1}-t_i)) - 1) \geq 0$  independently of the sign of  $b$ . This ends the proof.  $\blacksquare$

Figure 2 displays sample paths of  $(\widehat{V}, \widehat{U}, \widehat{Z})$  constructed using the iVi scheme in Algorithm 1 for  $a > 0$  (reflecting boundary) and  $a = 0$  (absorbing boundary). Notice how in both cases, all sample paths of  $\widehat{V}$  remain nicely nonnegative and  $\widehat{U}$  non-decreasing. For the first row,  $\widehat{V}$  bounces back when it reaches 0 while it gets absorbed at 0 for the second row.

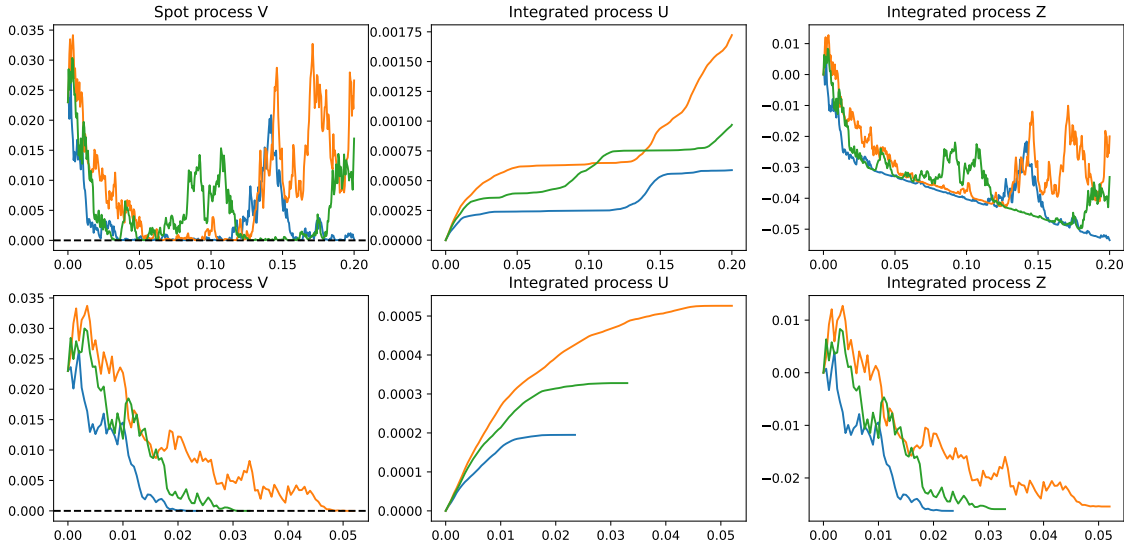


Figure 2: Row 1 - Reflecting boundary  $a > 0$ : Parameters as in Case 2 in Table 1 below. Row 2 - absorbing boundary:  $a = 0$  and other parameters unchanged.  $T = 0.2$  and a 400 time steps.

### 1.3 Distributional properties of the iVi scheme

The Inverse Gaussian distribution is not the only one satisfying (1.4), which naturally raises the question: *Why choose the Inverse Gaussian distribution?* In this section, we provide three justifications based on distributional properties of the square-root process:

- **First conditional moments** are perfectly captured for the processes  $(V, U, Z)$ , as shown in Proposition 1.4.
- **Discretization of the conditional characteristic function** of  $U$  naturally leads to an Inverse Gaussian distribution, see Proposition 1.5 and Remark 1.6.
- **Convergence of the process  $U$  towards an Inverse Gaussian process** happens in two configurations: (i) either in certain regimes with large mean reversion and volatility of volatility for any maturity (ii) or for large maturities independently of the other parameters, refer to Remark 1.7.

### 1.3.1 First conditional moments are matched

The next proposition shows that the first conditional moments of  $(V, U, Z)$  are perfectly matched by those of  $(\widehat{V}, \widehat{U}, \widehat{Z})$ . However, because of the approximation of the integral in (1.3), higher moments are not expected to be perfectly matched.

**Proposition 1.4.** *Fix  $i = 0, \dots, n - 1$  and  $v \geq 0$ . Then,*

$$\begin{aligned}\mathbb{E} [\widehat{U}_{i,i+1} \mid \widehat{V}_i = v] &= \mathbb{E} [U_{t_i, t_{i+1}} \mid V_i = v] = v \frac{e^{b(t_{i+1} - t_i)} - 1}{b} + \frac{a}{b} \left( \frac{e^{b(t_{i+1} - t_i)} - 1}{b} - (t_{i+1} - t_i) \right), \\ \mathbb{E} [\widehat{Z}_{i,i+1} \mid \widehat{V}_i = v] &= \mathbb{E} [Z_{t_i, t_{i+1}} \mid V_i = v] = 0, \\ \mathbb{E} [\widehat{V}_{i+1} \mid \widehat{V}_i = v] &= \mathbb{E} [V_{t_i} \mid V_i = v] = v e^{b(t_{i+1} - t_i)} + \frac{a}{b} (e^{b(t_{i+1} - t_i)} - 1).\end{aligned}$$

*Proof.* The explicit expressions for the conditional moments of  $(V, U, Z)$  are straightforward to obtain from (1.1), (0.2) and (1.2). Let us look at those of  $(\widehat{V}, \widehat{U}, \widehat{Z})$ . Conditional on  $\widehat{V}_i$ , it follows from (0.4) that  $\widehat{U}_{i,i+1}$  follows an Inverse Gaussian distribution with mean  $\alpha_i$ , see (A.2). Using the expression of  $\alpha_i$  in (0.3) we get

$$\mathbb{E} [\widehat{U}_{i,i+1} \mid \widehat{V}_i = v] = v \frac{e^{b(t_{i+1} - t_i)} - 1}{b} + \frac{a}{b} \left( \frac{e^{b(t_{i+1} - t_i)} - 1}{b} - (t_{i+1} - t_i) \right),$$

which proves the equality for the first moment of  $U$ . Using the construction of  $\widehat{Z}_{i,i+1}$  in (0.5) it follows that  $\mathbb{E} [\widehat{Z}_{i,i+1} \mid \widehat{V}_i = v] = 0$ , which shows the equality for the first moment of  $Z$ . Finally, using (0.6), we can compute

$$\begin{aligned}\mathbb{E} [\widehat{V}_{i+1} \mid \widehat{V}_i = v] &= v + a(t_{i+1} - t_i) + b\mathbb{E} [\widehat{U}_{i,i+1} \mid \widehat{V}_i = v] + c\mathbb{E} [\widehat{Z}_{i,i+1} \mid \widehat{V}_i = v] \\ &= v + a(t_{i+1} - t_i) + v(e^{b(t_{i+1} - t_i)} - 1) + a \left( \frac{e^{b(t_{i+1} - t_i)} - 1}{b} - (t_{i+1} - t_i) \right) \\ &= v e^{b(t_{i+1} - t_i)} + \frac{a}{b} (e^{b(t_{i+1} - t_i)} - 1),\end{aligned}$$

which proves the equality for the first moment of  $V$  and ends the proof.  $\blacksquare$

### 1.3.2 The distributions are intimately linked

To begin, the next proposition highlights striking similarities between the conditional characteristic functions of  $\widehat{U}$  and  $U$ : both exhibit an exponentially affine dependence on  $v$ . More importantly, the Inverse Gaussian distribution emerges naturally as an implicit Euler-type discretization of the Riccati equations governing the conditional characteristic function of  $U$  between two consecutive time steps. In what follows, we use the principal branch for the complex square-root.

**Proposition 1.5.** *Fix  $w \in \mathbb{C}$  such that  $\Re(w) \leq 0$ . Fix  $i = 0, \dots, n - 1$  and  $v \geq 0$ . Then,*

$$\mathbb{E} [\exp(w\widehat{U}_{i,i+1}) \mid \widehat{V}_i = v] = \exp(\widehat{\phi}_{i,i+1} + \widehat{\psi}_{i,i+1}v), \quad (1.6)$$

$$\mathbb{E} [\exp(wU_{t_i, t_{i+1}}) \mid V_i = v] = \exp(\phi(t_{i+1} - t_i) + \psi(t_{i+1} - t_i)v), \quad (1.7)$$

where

$$\widehat{\phi}_{i,i+1} = \frac{ac}{\sigma_i b} \left( \frac{e^{b(t_{i+1} - t_i)} - 1}{b} - (t_{i+1} - t_i) \right) \widehat{\psi}_{i,i+1} \quad \text{and} \quad \widehat{\psi}_{i,i+1} = \frac{1 - \sqrt{1 - 2w\sigma_i^2}}{c\sigma_i}, \quad (1.8)$$

with  $\sigma_i$  given by (0.3) and  $(\phi, \psi)$  are the functions explicitly given by (B.2). In particular,  $\widehat{\psi}_{i,i+1}$  is a root of the quadratic polynomial

$$\widehat{\psi} = w \frac{e^{b(t_{i+1}-t_i)} - 1}{b} + \frac{c\sigma_i}{2} \widehat{\psi}^2, \quad (1.9)$$

and  $(\phi, \psi)$  solve the equations

$$\phi(t) = a \int_0^t \psi(s) ds, \quad (1.10)$$

$$\psi(t) = w \frac{e^{bt} - 1}{b} + \frac{c^2}{2} \int_0^t e^{b(t-s)} \psi^2(s) ds, \quad t \geq 0. \quad (1.11)$$

*Proof.* We first prove (1.6) using the characteristic function of the Inverse Gaussian distribution recalled in (A.1). Conditional on  $\widehat{V}_i$ , it follows from (0.4) that  $\widehat{U}_{i,i+1}$  follows an Inverse Gaussian distribution with mean parameter  $\mu_i = \alpha_i$  and shape parameter  $\lambda_i = \frac{\alpha_i^2}{\sigma_i^2}$ . Then, (0.3) gives

$$\frac{\lambda_i}{\mu_i} = \frac{\alpha_i}{\sigma_i^2} = \widehat{V}_i \frac{1}{c\sigma_i} + \frac{a}{\sigma_i^2 b} \left( \frac{e^{b(t_{i+1}-t_i)} - 1}{b} - (t_{i+1} - t_i) \right) \quad \text{and} \quad \frac{\mu_i^2}{\lambda_i} = \sigma_i^2,$$

which plugged in (A.1) yields (1.6). In addition, it is straightforward to check that  $\widehat{\psi}_{i,i+1}$  solves (1.9). As for (1.7), it follows from the conditional characteristic function (B.1) applied with  $v = 0$  between  $t_i$  and  $t_{i+1}$ . In particular, a variation of constant formula on the Riccati equation for  $\psi$  in (B.3), with  $v = 0$ , yields (1.11). ■

With the help of Proposition 1.5, the choice of the Inverse Gaussian distribution can now be justified by a simple discretization of the Riccati equation (1.11) as follows.

**Remark 1.6.** *The first step is to discretize (1.11) using the right endpoint rule by writing  $\Delta_i = t_{i+1} - t_i$ :*

$$\psi(\Delta_i) \approx w \frac{e^{b\Delta_i} - 1}{b} + \frac{c^2}{2} \int_0^{\Delta_i} e^{b(\Delta_i-s)} ds \psi^2(\Delta_i) = w \frac{e^{b\Delta_i} - 1}{b} + \frac{c\sigma_i}{2} \psi^2(\Delta_i).$$

This yields the quadratic equation (1.9) as approximation for  $\psi(\Delta_i)$ . The root with a non-positive real part is given precisely by  $\widehat{\psi}_{i,i+1}$  in (1.8). As for  $\widehat{\phi}_{i,i+1}$  in (1.8), for small  $\Delta_i$  we have that

$$\widehat{\phi}_{i,i+1} \approx \frac{a\Delta_i}{2} \widehat{\psi}_{i,i+1},$$

which corresponds to a trapezoidal discretization of  $\phi(\Delta_i)$  in (1.10) with  $\psi(\Delta_i)$  being approximated by  $\widehat{\psi}_{i,i+1}$ . In other words, the discretization between  $t_i$  and  $t_{i+1}$  of the Riccati equations (1.10)-(1.11) that govern the conditional distribution of the integrated process  $U_{t_i, t_{i+1}}$  in (1.7) naturally leads to an Inverse Gaussian distribution of the form (1.6) and (1.8). ■

Another advantage of our scheme using the Inverse Gaussian distribution is that such distribution emerges as the limiting distribution of the integrated process  $U_{0,T}$  in two configurations:

**Remark 1.7.** • In market regimes characterized by high mean reversion and volatility of volatility: the results of [Mechkov \(2015\)](#) and later extended by [Abi Jaber and De Carvalho \(2024\)](#); [McCrickerd \(2019\)](#) have shown that under the parameterization  $c = -b\beta$  and  $a = -b\gamma$ , with  $\beta, \gamma > 0$ , as  $b \rightarrow \infty$ , the distribution of  $U_{0,T}$  converges to an Inverse Gaussian distribution. Furthermore, weak convergence holds for the entire process  $(U_{0,t})_{t \geq 0}$  towards an Inverse Gaussian Lévy process in Skorokhod spaces. This observation suggests that in such market regimes, which are typically encountered when calibrating the Heston model to the short end of the SPX volatility surface (see Figure 10), the iVi scheme is expected to perform exceptionally well. In particular, even with a minimal number of time steps—potentially as few as one single step—our approach maintains its accuracy, as already demonstrated in Figure 1.

- For large maturities, independently of the parameters, the limiting distribution of  $U_{0,T}$  as  $T \rightarrow \infty$  is also an Inverse Gaussian distribution as shown by [Forde and Jacquier \(2011\)](#). Interestingly, such limiting behavior has been used by [Tse and Wan \(2013\)](#) to justify the choice of an Inverse Gaussian distribution for the distribution of  $U_{t_i, t_{i+1}}$  conditional on the endpoints  $(V_{t_i}, V_{t_{i+1}})$  in Step 2 of the traditional approach recalled in the introduction. ■

## 2 Numerical illustrations for the integrated process $U$

In this section, we examine the performance of the iVi scheme given by Algorithm 1 for quantities involving the accumulated integrated process

$$U_{0,T} = \int_0^T V_s ds = \sum_{i=0}^{n-1} \int_{t_i}^{t_{i+1}} V_s ds = \sum_{i=0}^{n-1} U_{t_i, t_{i+1}},$$

which can be naturally approximated using our scheme by

$$\widehat{U}_{0,T} := \sum_{i=0}^{n-1} \widehat{U}_{t_i, t_{i+1}}.$$

We focus on the following three distributional quantities which also have a financial meaning:

1. **First moment:**  $\mathbb{E}[U_1]$ , which corresponds to the variance swap at maturity  $T = 1$  if  $U$  represents the integrated variance. The reference value is computed using:

$$\mathbb{E}[U_T] = V_0 \frac{e^{bT} - 1}{b} + \frac{a}{b} \left( \frac{e^{bT} - 1}{b} - T \right).$$

2. **Half-moment:**  $\mathbb{E}[\sqrt{U_1}]$ , representing the volatility swap. For the reference value, we use the inversion formula of the Laplace transform in [Schürger \(2002\)](#):

$$\mathbb{E}[\sqrt{U_1}] = \frac{1}{2\sqrt{\pi}} \int_0^\infty \frac{1 - \mathbb{E}[e^{-uU_1}]}{u^{3/2}} du,$$

where the Laplace transform is recalled in (B.1).

3. **Laplace transform:**  $\mathbb{E}[e^{-U_1}]$ , which can also be interpreted as the price of a zero-coupon bond if  $V$  models the short rate. The explicit reference value is recalled in (B.1).

The parameters for our tests are listed in Table 1. All three cases correspond to realistic parameter values. Cases 1 and 2 are derived from calibrating the Heston model to SPX market data on two distinct dates, October 10, 2017, and July 3, 2013. The fitted volatility surfaces are illustrated on Figures 9 and 10. Case 1 places an emphasis on short-dated options. Case 3, on the other hand, corresponds to the first case considered by [Andersen \(2008\)](#) and represents the market dynamics for long-dated FX options. The parameter  $\rho$  in Table 1 is not used in this section but will become relevant in the next section, where it is applied to the Heston model.

Case 1 is particularly challenging for simulation due to its high volatility of volatility and strong mean-reversion dynamics. Case 3 features relatively low mean-reversion compared to high volatility. Case 2 lies between the two extremes. In all three cases, the Feller condition is violated, i.e.  $a - \frac{c^2}{2} < 0$ .

For comparison, we also implement the Quadratic-Exponential (QE) scheme of [Andersen \(2008\)](#) and the second order scheme (AL) of [Alfonsi \(2010\)](#).

| Case          | $V_0$ | $a$                  | $b$    | $c$  | $\rho$ |
|---------------|-------|----------------------|--------|------|--------|
| <b>Case 1</b> | 0.006 | $17.25 \times 0.018$ | -17.25 | 2.95 | -0.68  |
| <b>Case 2</b> | 0.023 | $2.15 \times 0.057$  | -2.15  | 0.86 | -0.70  |
| <b>Case 3</b> | 0.04  | $0.5 \times 0.04$    | -0.5   | 1.0  | -0.9   |

Table 1: Parameter values for the three cases.

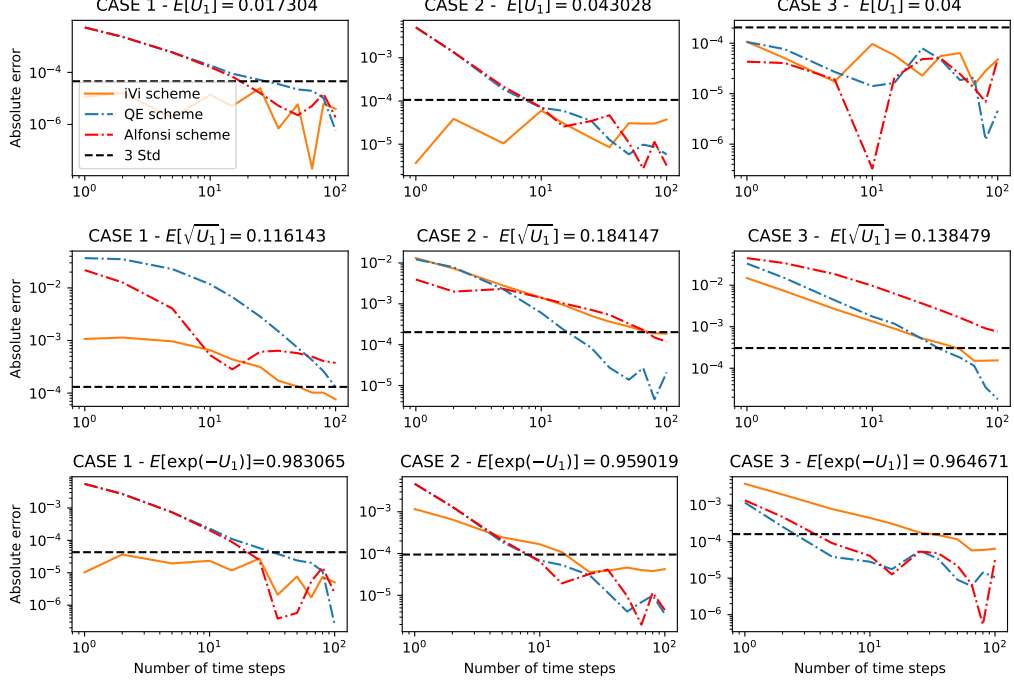


Figure 3: Errors on variance swaps, volatility swaps and Laplace transform of  $\hat{U}_T$  in terms of the number of time steps for the three cases with  $T = 1$  and 2 million sample paths.

Figure 3 shows the absolute error between the schemes and reference values varying number of time steps on a uniform grid from 1 to 100 in log-log scale. Simulations use 2 million sample paths. The horizontal black dotted line represents three standard deviations of the Monte Carlo estimator, below which comparisons can be considered non-significant. We can observe that:

- **Convergence:** All schemes converge as the number of time steps increases.
- **For  $\mathbb{E}[U_1]$ :** the iVi scheme achieves accuracy within three standard deviations across all cases, even with a single time step, in line with Proposition 1.4, outperforming the QE and AL schemes for the first two cases.
- **For Case 1:** the iVi scheme delivers highly accurate results for all quantities with a very small number of time steps, including  $\mathbb{E}[e^{-U_1}]$ , even with one single time step.
- **For Case 2:** The performance of the iVi scheme for the volatility swap and Laplace transform is comparable to other schemes, the iVi scheme is more accurate when we have less than 5 time steps in 4 out of the 6 cases.
- **For Case 3:** The QE and AL schemes converge faster for the Laplace transform.

To sum up, for quantities on the integrated process  $U$ , the iVi scheme converges and competes favorably with the QE and AL schemes, particularly in challenging regimes with high volatility-of-volatility and strong mean reversion.

### 3 Numerical illustrations for the Heston model

In this section, we test our iVi scheme on the [Heston \(1993\)](#) model where the stock price  $S$  is given by

$$dS_t = S_t \sqrt{V_t} \left( \rho dW_t + \sqrt{1 - \rho^2} dW_t^\perp \right), \quad S_0 > 0, \quad (3.1)$$

where  $V$  is given by [\(0.1\)](#),  $\rho \in [-1, 1]$  and  $W^\perp$  is a standard Brownian motion independent of  $W$ .

In order to simulate  $S$  it suffices to observe that

$$\log S_{t_{i+1}} = \log S_{t_i} - \frac{1}{2} U_{t_i, t_{i+1}} + \rho Z_{t_i, t_{i+1}} + \sqrt{1 - \rho^2} \int_{t_i}^{t_{i+1}} \sqrt{V_s} dW_s^\perp,$$

and that conditional on  $U_{i, i+1}$ ,  $\int_{t_i}^{t_{i+1}} \sqrt{V_s} dW_s^\perp \sim \mathcal{N}(0, U_{t_i, t_{i+1}})$ , for  $i = 0, \dots, n - 1$ .

We can therefore simulate  $(\log \hat{S}_i)_{i=0, \dots, n}$  using the outputs  $(\hat{U}, \hat{Z})$  of Algorithm [\(1\)](#) using:

$$\begin{aligned} \log \hat{S}_0 &= \log S_0, \\ \log \hat{S}_{i+1} &= \log \hat{S}_i - \frac{1}{2} \hat{U}_{i, i+1} + \rho \hat{Z}_{i, i+1} + \sqrt{1 - \rho^2} \sqrt{\hat{U}_{i, i+1}} N_i, \quad i = 0, \dots, n - 1, \end{aligned} \quad (3.2)$$

where  $(N_i)_{i=0, \dots, n-1}$  are i.i.d. standard Gaussian random variables.

Clearly, the update rule [\(3.2\)](#) at the  $i$ -th step  $i$  can be incorporated in Algorithm [1](#) right after [\(0.6\)](#). Also, the  $(N_i)_{i=0, \dots, n-1}$  need to be taken independent from the Gaussian and Uniform random variables used for the sampling of the Inverse Gaussian distribution in Algorithm [2](#).

For our numerical experiment, we will consider call options on  $S$  for the three cases of Table [1](#) with maturity  $T = 1$  for the first cases and the longer maturity  $T = 10$  for the third case. Reference values are computed using Fourier inversion techniques on the characteristic function of the log-price which is known explicitly in the Heston model, see [\(B.1\)](#). Simulations use 2 million sample paths and we also benchmark against the QE and AL schemes.

Figure [4](#) displays the absolute error between the schemes and reference values varying number of time steps from 1 to 100 in log-log scale for In-the-Money (ITM), At-the-Money (ATM) and Out-of-The-Money (OTM). We can again observe the convergence of the iVi scheme. For ITM call option, the iVi scheme yields a fast convergence (compared to QE and AL schemes) in all three cases. Again, for Case 1, our scheme achieves accuracy within three standard deviations with a single time step, in line with Figure [3](#). For ATM and OTM call options, as the strike increases, the convergence speed seems to deteriorate for our scheme (compared to the QE scheme). Still for case 1 (first column), our scheme achieves accurate results with one single time step.

Figures [5](#), [6](#), and [7](#) display the full implied volatility slices for the three cases, corresponding to simulations with 1, 5, and 15 time steps. These figures also include the absolute errors in implied volatility and the mean absolute errors across the entire slice. The iVi scheme demonstrates excellent accuracy with just 1 and 5 time steps, particularly for Case 1. With 15 time steps, the slices of the iVi scheme and the reference values become nearly indistinguishable for all three cases. Compared to the QE and AL schemes, the iVi scheme is always more accurate for (deep) ITM call options, and for the whole volatility slice our scheme outperforms, in terms of Mean Absolute Error (MAE), for 7 out of the 9 plots.

Additionally, for Case 1, Figure [1](#) provides six slices of the volatility surface, computed using the iVi scheme with only a single time step per slice, highlighting the scheme's efficiency in approximating the entire surface with minimal discretization in high mean-reversion and volatility-of-volatility market regimes.

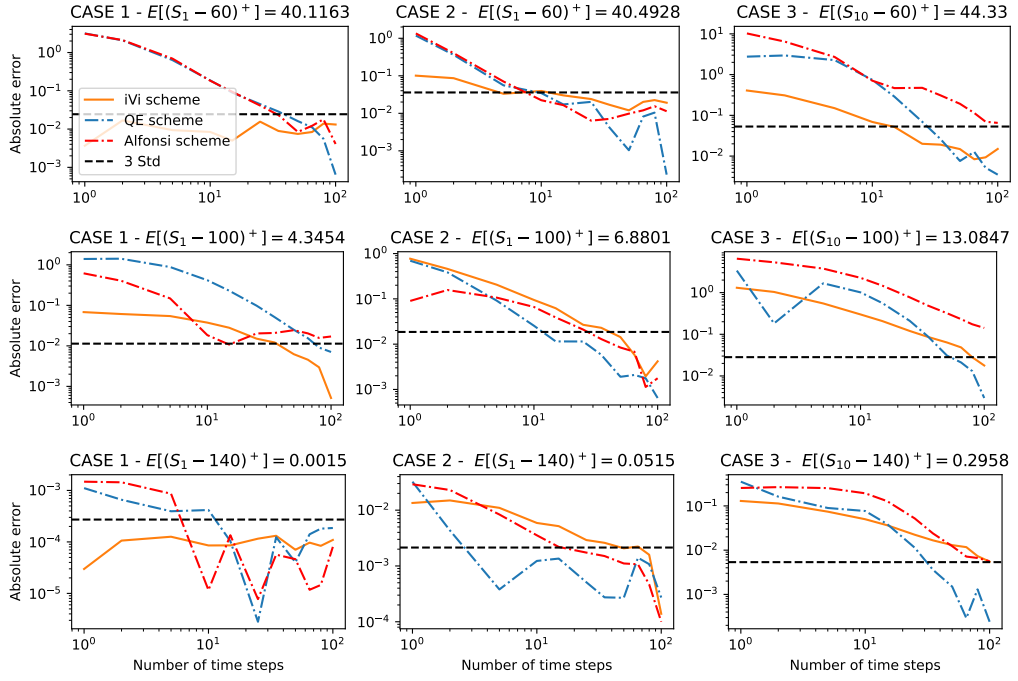


Figure 4: ITM, ATM and OTM call options on  $S$ : error in prices in terms of number of time steps for the three cases with 2 million sample paths.

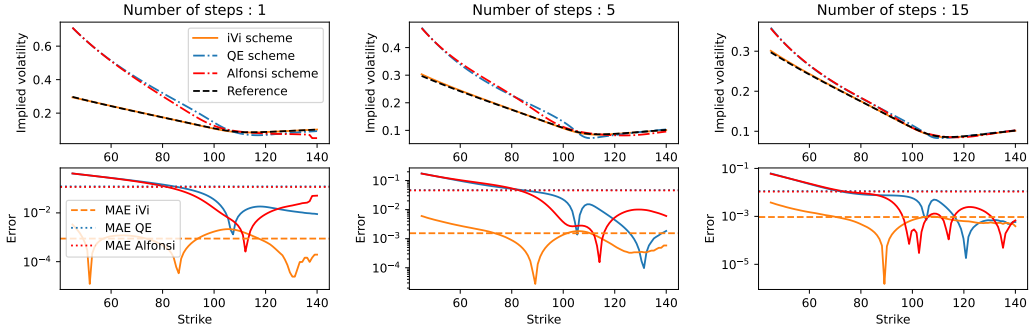


Figure 5: **Case 1:** Implied volatility slice for  $T = 1$  and 2 million sample paths.

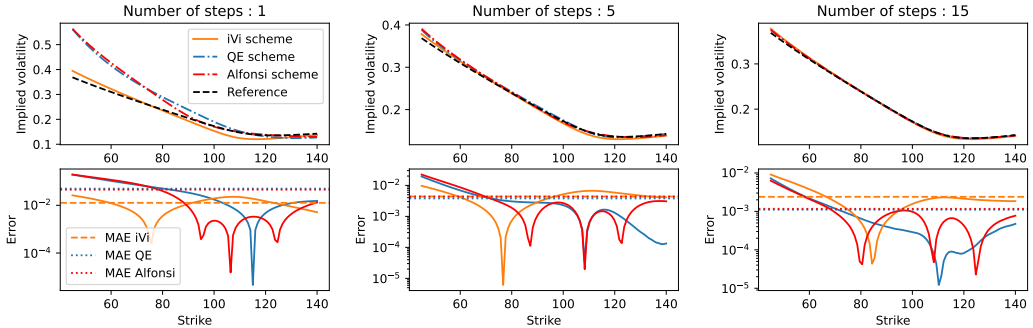


Figure 6: **Case 2:** Implied volatility slice for  $T = 1$  and 2 million sample paths.

Finally, to illustrate the relevance of the iVi scheme for practical applications, for instance, when the Heston model is used as a component of a Local Stochastic Volatility model, a small number of

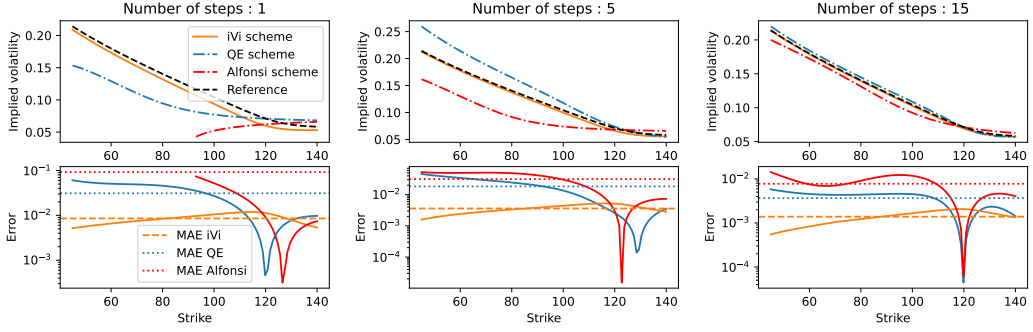


Figure 7: **Case 3:** Implied volatility slice for  $T = 10$  and 2 million sample paths.

paths is typically used with a fixed number of time steps. Figure 8 shows the option prices obtained from the three schemes using fewer paths (ranging from 10k to 200k) with 50 time steps. Among the three schemes, the iVi scheme appears to produce the most stable results across different numbers of sample paths.

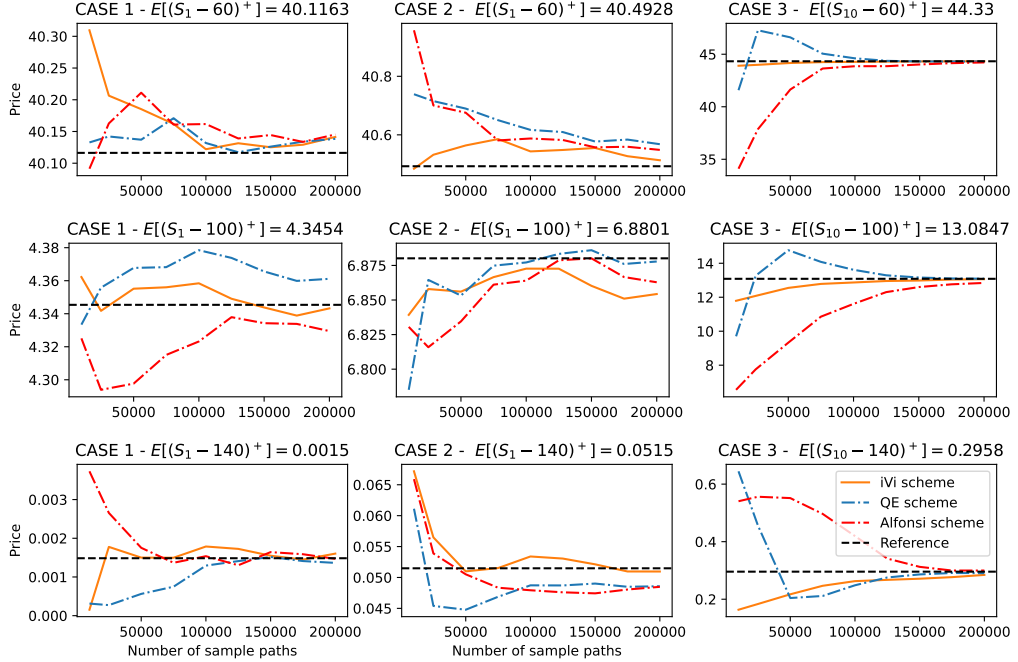


Figure 8: ITM, ATM and OTM call options on  $S$ : prices in terms of the number of sample paths for the three cases with 50 time steps.

All in all, the iVi scheme seems pretty competitive across several parameter sets, strikes and maturities when pricing call options in the Heston model, especially with a little number of time steps. It is worth noting that second and third-order schemes of [Alfonsi \(2010\)](#), as well as the QE scheme, all rely on switching mechanisms, which can be less robust, especially in the high volatility-of-volatility and fast mean-reversion regimes. In contrast, the iVi scheme already incorporates the Inverse Gaussian limiting distribution in such regimes, and appears to perform more reliably, without the need of switching mechanisms.

## 4 Extensions

Extension of the method to multivariate settings, even in affine models such as Wishart-type processes, is not straightforward. The Inverse Gaussian distribution used here is inherently one-dimensional, and extending it to higher dimensions while preserving tractability appears nontrivial. However, the scheme does naturally extend to path-dependent settings and can be used to efficiently simulate classes of Volterra and rough Heston models. This has been developed very recently in [Abi Jaber and Attal \(2025\)](#). In particular, ([Abi Jaber and Attal, 2025](#), Theorem 2.2 and Corollary 2.3) guarantee the theoretical convergence of the iVi scheme.

## A Inverse Gaussian and its sampling

The Inverse Gaussian distribution, also known as the Wald distribution, is a continuous probability distribution on  $\mathbb{R}_+$  with two parameters:  $\mu > 0$  (mean parameter) and  $\lambda > 0$  (shape parameter). The probability density function of the Inverse Gaussian distribution is given by:

$$f(x; \mu, \lambda) = \sqrt{\frac{\lambda}{2\pi x^3}} \exp\left(-\frac{\lambda(x - \mu)^2}{2\mu^2 x}\right), \quad x > 0.$$

We denote  $X \sim IG(\mu, \lambda)$  to indicate that  $X$  is a random variable with an inverse Gaussian distribution with mean parameter  $\mu$  and shape parameter  $\lambda$ . Its characteristic function is given by

$$\mathbb{E}[\exp(wX)] = \exp\left(\frac{\lambda}{\mu}\left(1 - \sqrt{1 - \frac{2w\mu^2}{\lambda}}\right)\right), \quad (\text{A.1})$$

for all  $w \in \mathbb{C}$  such that  $\Re(w) \leq 0$ . In addition, its mean is given by

$$\mathbb{E}[X] = \mu. \quad (\text{A.2})$$

Inverse Gaussian random variables can be simulated easily using one Gaussian random variable and one Uniform random variable using an acceptance-rejection step as shown in [Michael, Schucany, and Haas \(1976\)](#), we recall the algorithm here.

---

### Algorithm 2 Sampling from the Inverse Gaussian Distribution

---

- 1: **Input:** Parameters  $\mu > 0$ ,  $\lambda > 0$ .
- 2: **Output:** Sample  $IG$  from the Inverse Gaussian distribution.
- 3: Generate  $\xi \sim \mathcal{N}(0, 1)$  and compute  $Y = \xi^2$ .
- 4: Compute the candidate value  $X$ :

$$X = \mu + \frac{\mu^2 Y}{2\lambda} - \frac{\mu}{2\lambda} \sqrt{4\mu\lambda Y + \mu^2 Y^2}.$$

- 5: Generate a uniform random variable: Sample  $\eta \sim \text{Uniform}(0, 1)$ .
  - 6: Select the output:
  - 7: **if**  $\eta \leq \frac{\mu}{\mu + X}$  **then**
  - 8:     Set the output  $IG = X$ .
  - 9: **else**
  - 10:    Set  $IG = \frac{\mu^2}{X}$ .
  - 11: **end if**
-

## B Heston's characteristic function

We recall the expression of the joint characteristic function of the integrated variance  $U_{t,T} = \int_t^T V_s ds$  and  $\log S$  in the [Heston \(1993\)](#) model in (3.1) with  $V$  given by (0.1). Let  $u, w \in \mathbb{C}$  be such that

$$\Re w + \frac{1}{2} ((\Re u)^2 - \Re u) \leq 0.$$

The joint conditional characteristic function of  $(\log S, U)$  is given by

$$\mathbb{E} \left[ \exp \left( u \log \frac{S_T}{S_t} + w U_{t,T} \right) \middle| V_t \right] = \exp (\phi(T-t) + \psi(T-t) V_t), \quad t \leq T, \quad (\text{B.1})$$

where  $(\phi, \psi)$  are explicitly given by

$$\begin{aligned} \psi(t) &= \frac{\beta(u) - D(u, w)}{c^2} \frac{1 - e^{-D(u, w)t}}{1 - G(u, w)e^{-D(u, w)t}}, \\ \phi(t) &= \frac{a}{c^2} \left( (\beta(u) - D(u, w))t - 2 \log \left( \frac{G(u, w)e^{-D(u, w)t} - 1}{G(u, w) - 1} \right) \right), \quad t \geq 0, \\ \beta(u) &= -b - u\rho c, \quad D(u, w) = \sqrt{\beta(u)^2 + c^2(-2w + u - u^2)}, \quad G(u, w) = \frac{\beta(u) - D(u, w)}{\beta(u) + D(u, w)}. \end{aligned} \quad (\text{B.2})$$

In particular,  $(\phi, \psi)$  solve the following system of Riccati equations

$$\begin{aligned} \phi'(t) &= a\psi(t), \quad \phi(0) = 0, \\ \psi'(t) &= \frac{c^2}{2}\psi^2(t) + (\rho cu + b)\psi(t) + w + \frac{u^2 - u}{2}, \quad \psi(0) = 0. \end{aligned} \quad (\text{B.3})$$

See for example ([Abi Jaber and De Carvalho, 2024](#), Theorem 2.1) and ([Gatheral, 2011](#), Chapter 2), [Albrecher et al. \(2007\)](#) for the explicit derivation of the formulas, and [Heston \(1993\)](#) for the initial derivation.

## C Calibrated volatility surfaces on SPX data

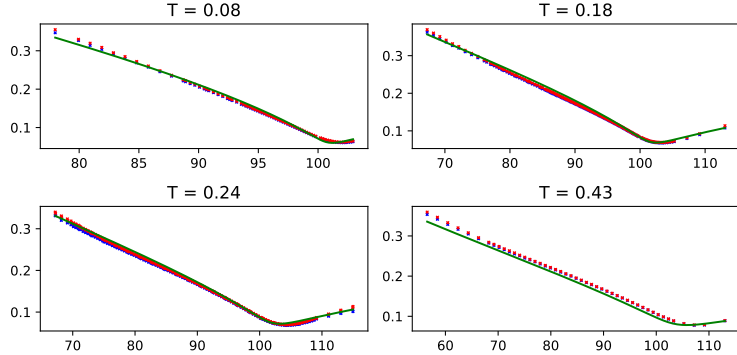


Figure 9: Implied volatility surface of the calibrated Heston model (green) on the market bid and ask implied volatilities (red and blue dots) on October 10, 2017. Calibrated parameters correspond to Case 1 in Table 1. Market data from the CBOE website <https://datashop.cboe.com/>.

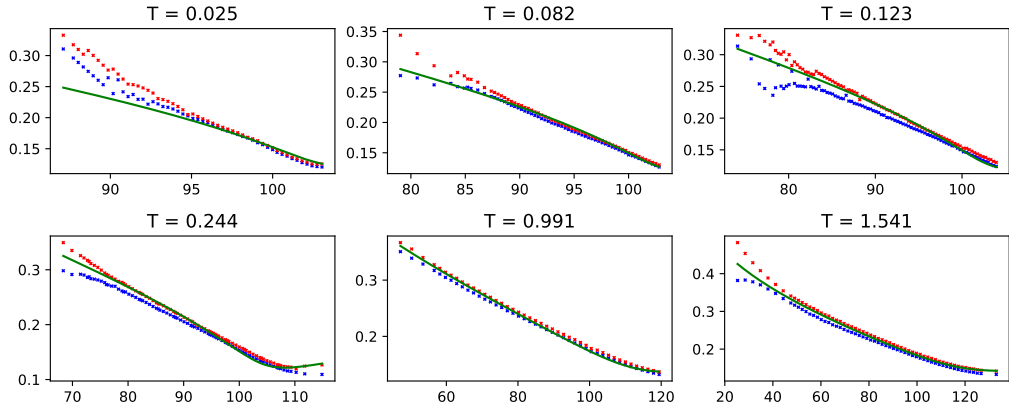


Figure 10: Implied volatility surface of the calibrated Heston model (green) on the market bid and ask implied volatilities (red and blue dots) on July 3, 2013. Calibrated parameters correspond to Case 2 in Table 1. Market data from the CBOE website <https://datashop.cboe.com/>.

## References

- Eduardo Abi Jaber and Elie Attal. Simulating integrated Volterra square-root processes and Volterra Heston models via Inverse Gaussian. *arXiv preprint arXiv:2504.19885*, 2025.
- Eduardo Abi Jaber and Nathan De Carvalho. Reconciling rough volatility with jumps. *SIAM Journal on Financial Mathematics*, 15(3):785–823, 2024.
- Hansjörg Albrecher, Philipp Mayer, Wim Schoutens, and Jurgen Tistaert. The little Heston trap. *Wilmott*, (1):83–92, 2007.
- Aurélien Alfonsi. On the discretization schemes for the CIR (and Bessel squared) processes. *Monte Carlo Methods Appl.*, 11(4):355–384, 2005.
- Aurélien Alfonsi. High order discretization schemes for the CIR process: application to affine term structure and Heston models. *Mathematics of computation*, 79(269):209–237, 2010.
- Leif Andersen. Simple and efficient simulation of the Heston stochastic volatility model. *Journal of Computational Finance*, 11(3):1–43, 2008.
- Jean-François Bégin, Mylène Bédard, and Patrice Gaillardetz. Simulating from the Heston model: A gamma approximation scheme. *Monte Carlo Methods and Applications*, 21(3):205–231, 2015.
- Abdel Berkaoui, Mireille Bossy, and Awa Diop. Euler scheme for SDEs with non-Lipschitz diffusion coefficient: strong convergence. *ESAIM: Probability and Statistics*, 12:1–11, 2008.
- Mark Broadie and Özgür Kaya. Exact simulation of stochastic volatility and other affine jump diffusion processes. *Operations research*, 54(2):217–231, 2006.
- Jaehyuk Choi and Yue Kuen Kwok. Simulation schemes for the Heston model with Poisson conditioning. *European Journal of Operational Research*, 314(1):363–376, 2024.
- John C Cox, Jonathan E Ingersoll Jr, and Stephen A Ross. A theory of the term structure of interest rates. *Econometrica: Journal of the Econometric Society*, pages 385–407, 1985.
- Griselda Deelstra and Freddy Delbaen. Convergence of discretized stochastic (interest rate) processes with stochastic drift term. *Applied stochastic models and data analysis*, 14(1):77–84, 1998.
- Darrell Duffie and Kenneth J Singleton. Credit risk: pricing, measurement, and management. In *Credit Risk*. Princeton university press, 2012.

- Darrell Duffie, Damir Filipović, and Walter Schachermayer. Affine processes and applications in finance. *The Annals of Applied Probability*, 13(3):984–1053, 2003.
- Martin Forde and Antoine Jacquier. The large-maturity smile for the Heston model. *Finance and Stochastics*, 15(4):755–780, 2011.
- J Gatheral. *The volatility surface: A Practitioner’s Guide*. John Wiley and Sons, Inc, 2011.
- Paul Glasserman and Kyoung-Kuk Kim. Gamma expansion of the Heston stochastic volatility model. *Finance and Stochastics*, 15:267–296, 2011.
- István Gyöngy and Miklós Rásonyi. A note on Euler approximations for SDEs with Hölder continuous diffusion coefficients. *Stochastic processes and their applications*, 121(10):2189–2200, 2011.
- Steven L Heston. A closed-form solution for options with stochastic volatility with applications to bond and currency options. *The review of financial studies*, 6(2):327–343, 1993.
- Desmond J Higham and Xuerong Mao. Convergence of Monte Carlo simulations involving the mean-reverting square root process. *Journal of Computational Finance*, 8(3):35–61, 2005.
- Christian Kahl and Peter Jäckel. Fast strong approximation Monte Carlo schemes for stochastic volatility models. *Quantitative Finance*, 6(6):513–536, 2006.
- Gytenis Lileika and Vigirdas Mackevičius. Weak approximation of CKLS and CEV processes by discrete random variables. *Lithuanian Mathematical Journal*, 60:208–224, 2020.
- Ryan McCrickerd. On spatially irregular ordinary differential equations and a pathwise volatility modelling framework. *arXiv preprint arXiv:1902.01673*, 2019.
- Serguei Mechkov. Fast-reversion limit of the Heston model. *Available at SSRN 2418631*, 2015.
- John R Michael, William R Schucany, and Roy W Haas. Generating random variates using transformations with multiple roots. *The American Statistician*, 30(2):88–90, 1976.
- Andreas Neuenkirch and Lukasz Szpruch. First order strong approximations of scalar SDEs defined in a domain. *Numerische Mathematik*, 128:103–136, 2014.
- Dylan Possamaï and Pierre Gauthier. Efficient simulation of the double Heston model. *The IUP Journal of Computational Mathematics*, 4(3):23–73, 2011.
- Daniel Revuz and Marc Yor. *Continuous martingales and Brownian motion*, volume 293. Springer Science & Business Media, 2013.
- Klaus Schürger. Laplace transforms and suprema of stochastic processes. *Advances in finance and stochastics: essays in honour of Dieter Sondermann*, pages 285–294, 2002.
- Shu Tong Tse and Justin WL Wan. Low-bias simulation scheme for the Heston model by Inverse Gaussian approximation. *Quantitative finance*, 13(6):919–937, 2013.
- Alexander Van Haastrecht and Antoon Pelsser. Efficient, almost exact simulation of the Heston stochastic volatility model. *International Journal of Theoretical and Applied Finance*, 13(01):1–43, 2010.
- Jianwei Zhu. A simple and accurate simulation approach to the Heston model. *Journal of Derivatives*, 18(4):26, 2011.